Table 1: HHV of Ethanol, *i*-pentanol, and Gasoline

Compound	Ethanol [1]	*i*-pentanol[1]	Gasoline [2]
HHV [MJ/kg]	29.67	37.73	48.46

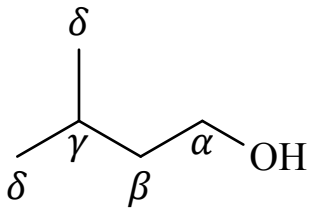

Figure 1: Skeletal structure of *i*-pentanol

0.1 Structure of *i*-Pentanol

i-Pentanol (3-methyl-1-butanol) is a five-carbon alcohol whose skeletal structure is shown in Fig. 1. *i*-Pentanol can be produced biologically, and offers several similar advantages as the butanol isomers as compared to ethanol. Table 1 compares the HHV of ethanol, *i*-pentanol, and gasoline.

0.2 Procedures

Experiments for *i*-pentanol in the RCM have been performed at the conditions listed in Table 2. Homogeneous fuel and air pre-mixtures are prepared in an approximately 17 L mixing tank. The mixing tank and all tubes and manifolds connecting the tank with the RCM are heated, allowing the study of relatively low vapor pressure fuels. The initial temperature is set above the saturation temperature of *i*-pentanol for each mixture studied. The mixing tank is equipped with a magnetic stirrer to ensure complete homogeneity of the mixture.

Prior to mixture preparation, the mixing tank is vacuumed to less than 1 Torr, whereupon liquid fuel (*i*-pentanol, Sigma-Aldrich, 99.6% purity) is injected by a syringe through a septum. The syringe is massed before and after the injection, with the difference being the amount of fuel in the mixing tank. Based on this mass, required proportions of the gaseous oxidizer (O2, 99.994% purity, N2, 99.999% purity) are calculated. The gases are added to the mixing tank sequentially at room temperature and the total pressure is monitored to ensure the proper mixture concentra-

Table 2: *i*-pentanol Experimental Conditions

Reactant (Purity)			Equivalence Ratio ϕ	Compressed Pressure P_C (bar)
i-pentanol (99.6%)	O_2 (99.994%)	N_2 (99.999%)		
Mole Percentage				
2.41	20.50	77.09	1.0	7
2.41	20.50	77.09	1.0	20
2.41	20.50	77.09	1.0	40
1.22	20.75	78.03	0.5	7
1.22	20.75	78.03	0.5	20
1.22	20.75	78.03	0.5	40
4.71	20.01	75.27	2.0	20
4.71	20.01	75.27	2.0	40

tions are attained. Finally, the heaters and stirring vane are switched on and the system is allowed approximately 1.5 h to reach steady state.

0.3 Model Improvements

Through collaboration with researchers at Lawrence Livermore National Laboratory, many improvements to the chemical kinetic model for *i*-pentanol were made relative to the work of Tsujimura et al. [3]. Some of the major improvements are highlighted below; see the article for more detail [4].

1. The model was restructured based on work with C_4 and C_5 alcohols [5, 6]
2. The most stable conformers of *i*-pentanol were calculated using quantum chemistry software
3. The BDEs of the of the C-C, C-H, C-O, and O-H bonds were calculated using quantum chemistry software
4. The model includes the Waddington pathway shown to be important in low-temperature decomposition of *i*-pentanol by Welz et al. [7]

5. New reaction pathways were added based on the work of Welz et al. [7, 8], including the unconventional water-elimination pathway discussed in Welz et al. [8]

Moreover, the following data sets from the literature and presented in [4] were used to validate the newly updated model, in addition to the data presented here.

1. Ignition delays measured in a shock tube [3, 9]
2. JSR species data [10]
3. New ignition delays measured in shock tubes [4]
4. New JSR species data [4]
5. New flame speed and flame extinction measurements [4]

0.4 Experimental & Modeling Results

The experimental ignition delays measured in the RCM are shown in Figs. 5, 6, and 7, along with ignition delays measured in the shock tube and comparison with the model simulations. There is no $\phi = 2.0$ data set for 7 atm because no conditions at which ignition occurred could be found. In Figs. 5–7, solid lines represent adiabatic, constant volume simulations, and dashed lines represent volume-profile simulations.

At 7 atm, the high-temperature ignition delays are generally predicted to within a factor of 1.5. The RCM experiments are also well predicted at low temperature—within a factor of 2—but the disagreement grows to approximately a factor of 4 in the intermediate temperature regime. At 20 atm, the high-temperature ignition delays are well predicted, including capturing the equivalence ratio sensitivity of the ignition delays. The ignition delays measured in the RCM are fairly well predicted at the lean and stoichiometric condition, but are over-predicted at the rich condition.

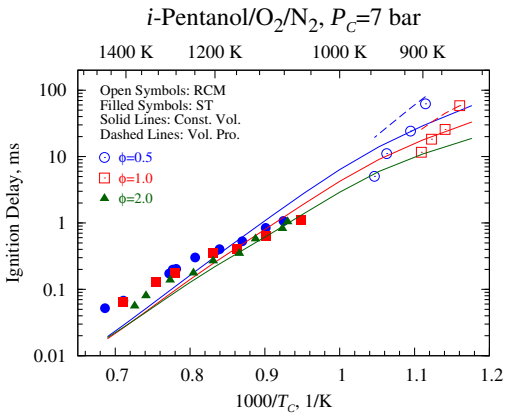

Figure 2: Shock tube and RCM ignition delay times from Tsujimura et al. [3] at 7 atm compared with model predictions by the model from Sarathy et al. [4].

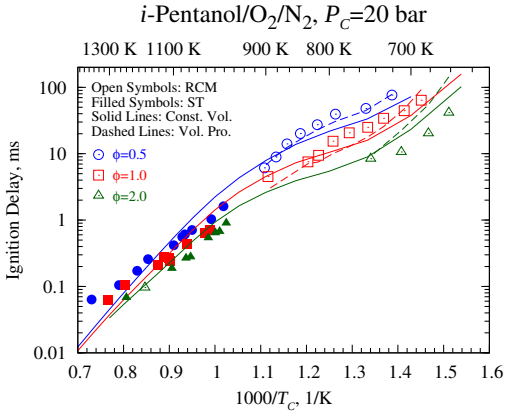

Figure 3: Shock tube and RCM ignition delay times from Tsujimura et al. [3] at 20 atm compared with model predictions by the model from Sarathy et al. [4].

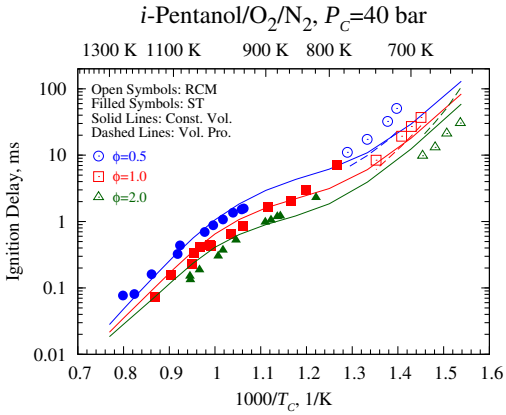

Figure 4: Shock tube and RCM ignition delay times from Sarathy et al. [4] at 40 atm compared with model predictions by the model from Sarathy et al. [4].

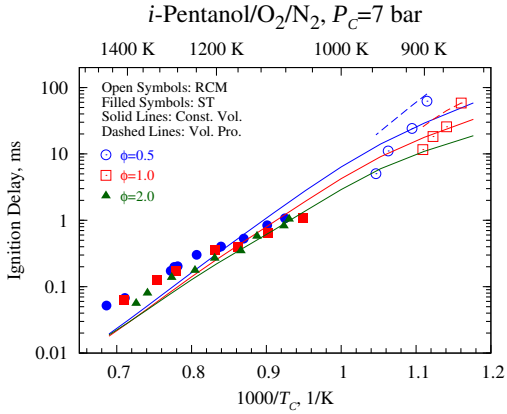

Figure 5: Shock tube and RCM ignition delay times from Tsujimura et al. [3] at 7 atm compared with model predictions by the model from Sarathy et al. [4].

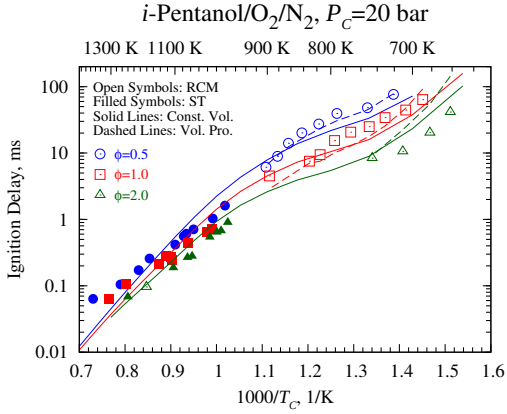

Figure 6: Shock tube and RCM ignition delay times from Tsujimura et al. [3] at 20 atm compared with model predictions by the model from Sarathy et al. [4].

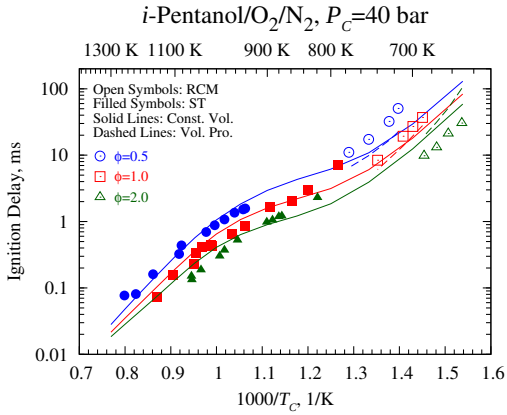

Figure 7: Shock tube and RCM ignition delay times from Sarathy et al. [4] at 40 atm compared with model predictions by the model from Sarathy et al. [4].